Contract No:

This document was prepared in conjunction with work accomplished under Contract No. DE-AC09-08SR22470 with the U.S. Department of Energy (DOE) Office of Environmental Management (EM).

Disclaimer:

DESTRUCTIVE EXAMINATION OF SHIPPING PACKAGE 9975-02019

W. L. Daugherty

June 2016

SRNL-STI-2016-00324, Revision 0

DISCLAIMER

Printed in the United States of America

Prepared for
U.S. Department of Energy

SRNL-STI-2016-00324
Revision 0

Keywords: *K-Area*
Surveillance
9975 Shipping Package

Retention: *Permanent*

DESTRUCTIVE EXAMINATION OF SHIPPING PACKAGE 9975-02019

W. L. Daugherty

June 2016

Prepared in conjunction with work accomplished under contract number DE-AC09-08SR22470 with the U.S. Department of Energy (DOE) Office of Environmental Management (EM).

DESTRUCTIVE EXAMINATION OF SHIPPING PACKAGE 9975-02019

APPROVALS:

W. L. Daugherty _____ Date _____
Author, Materials Science and Technology

T. E. Skidmore _____ Date _____
Technical Review, Materials Science and Technology

B. L. Garcia-Diaz _____ Date _____
Pu Surveillance Program Lead, Materials Science and Technology

K. E. Zeigler _____ Date _____
Manager, Materials Science and Technology

E. R. Hackney _____ Date _____
NMM Engineering

REVIEWS:

D. R. Leduc _____ Date _____
Savannah River Packaging Technology

J. W. McEvoy _____ Date _____
9975 Shipping Package Design Authority

Summary

Destructive and non-destructive examinations have been performed on the components of shipping package 9975-02019 as part of a comprehensive SRS surveillance program for plutonium material stored in the K-Area Complex (KAC). During the field surveillance inspection of this package in KAC, two non-conforming conditions were noted: the axial gap of 1.577 inch exceeded the 1 inch maximum criterion, and two areas of dried glue residue were noted on the upper fiberboard subassembly.

This package was subsequently transferred to SRNL for more detailed inspection and destructive examination. In addition to the conditions noted in KAC, the following conditions were noted:

- Numerous small spots of corrosion were observed along the bottom edge of the drum.
- In addition to the smeared glue residue on the upper fiberboard subassembly, there was also a small dark stain.
- Mold was present on the side and bottom of the lower fiberboard subassembly. Dark stains from elevated moisture content were also present in these areas.
- A dark spot with possible light corrosion was observed on the primary containment vessel flange, and corresponding rub marks were observed on the secondary containment vessel ID.
- The fiberboard thermal conductivity in the radial orientation was above the specified range. When the test was repeated with slightly lower moisture content, the result was acceptable. The moisture content for both tests was within a range typical of other packages in storage.

The observed conditions must be fully evaluated by KAC to ensure the safety function of the package is being maintained.

Several factors can contribute to the concentration of moisture in the fiberboard, including higher than average initial moisture content, higher internal temperature (due to internal heat load and placement within the array of packages), and the creation of additional moisture as the fiberboard begins to degrade.

Introduction

The Savannah River Site (SRS) stores packages containing plutonium (Pu) materials in the K-Area Complex (KAC). The Pu materials are packaged per the DOE 3013 Standard and stored within Model 9975 shipping packages in KAC.

The KAC facility DSA (Documented Safety Analysis) [1] credits the Model 9975 package to perform several safety functions, including criticality prevention, impact resistance, containment, and fire resistance to ensure the plutonium materials remain in a safe configuration during normal and accident conditions. The Model 9975 package is expected to perform its safety function for at least 15 years in the storage environment [2]. The DSA recognizes the degradation potential for the materials of package construction over time in the KAC storage environment and requires an assessment of materials performance to validate the assumptions of the analysis. This assessment is documented in the SRS Site Surveillance Program which is used to monitor material performance in order to establish a basis for the service life.

As part of the Site Surveillance Program [3-4], destructive examination of package 9975-02019 was performed following field surveillance in accordance with Reference 5. Field surveillance of the Model 9975 package in KAC included nondestructive examination of the drum, fiberboard, lead shield and containment vessels [4, 6]. Results of the field surveillance are provided in Attachment 1.

Package History

Package 9975-02019 was loaded with plutonium oxide material packaged at RFETS in accordance with DOE-STD-3013 and received into KAC in June 2003. The contents generated approximately 14.6 watts heat load. Routine field surveillance was performed on April 5, 2016. After transfer to SRNL, DE examination activities were performed between April 20 and May 19, 2016.

Discussion

The results of the field surveillance [7] were reviewed. Two items were identified as unsatisfactory in the field surveillance:

- Dried glue residue was observed on two areas of the upper fiberboard subassembly.
- The axial gap (1.577 inch) exceeded the 1 inch maximum criterion.

As the package was first opened in SRNL and components removed, each component was marked to identify its orientation within the package. For components that were removed during the field surveillance, their orientation at the time of this examination probably bears no relation to their orientation while stored in KAC. However, the bottom fiberboard subassembly and lead shield would likely have remained in the same orientation they occupied in KAC.

Examination activities are documented through photographs, data sheets, and other documents. This documentation is maintained in a laboratory notebook [8]. The following examination activities were performed:

Fiberboard physical properties:

The weight and dimensions of the top and bottom fiberboard subassemblies were measured. The weight of the top subassembly was 12.129 kg (26.74 lb). During the field surveillance, the measured weight of the top subassembly was 26.8 lb. These two values are in good agreement. Weight and dimension data are recorded in Table 1.

The air shield was cut and peeled back at four locations to permit accurate measurement of the top fiberboard subassembly dimensions. In order to calculate the density of each subassembly, nominal dimensions were assumed for the air shield and aluminum bearing plates. The calculated densities (0.273 g/cc top subassembly, 0.298 g/cc bottom subassembly) meet the limit for the criticality control function, 0.20 g/cc minimum [5]. The volume and density were calculated using the following equations (see the Table 1 sketch for dimension nomenclature).

$$\text{Top subassembly fiberboard volume, } V_U = (UD1)^2\,(UH1)\,(\pi/4) + [(UD1) - 2\,(UR2)]^2\,(UH2)\,(\pi/4) - (UD2)^2\,(UH3)\,(\pi/4) - 59.96\ \text{inch}^3$$

Top subassembly fiberboard weight, W_U = upper subassembly weight – 9.773 lb
Top subassembly fiberboard density, $\rho_U = W_U / V_U$
Bottom subassembly fiberboard volume, $V_L = (LD1)^2 (LH1) (\pi/4) - [(LD2) + 2 (LR1)]^2 (LH3) (\pi/4) - (LD2)^2 (LH2) (\pi/4) – 59.96$ inch^3
Bottom subassembly fiberboard weight, W_L = bottom subassembly weight – 4.827 lb
Bottom subassembly fiberboard density, $\rho_L = W_L / V_L$

Fiberboard dimensions measured during field surveillance are summarized in Attachment 1, and are generally consistent with drawing requirements and destructive examination measurements. For each of the dimensions measured in both the field surveillance and destructive examination, the measured values are similar. The dimensions were measured in SRNL 15 days after the field surveillance.

The axial gap measured during field surveillance (1.577 inch) did not meet the specified 1 inch maximum criterion, and was slightly larger when measured in SRNL (1.630 inch). The increase likely resulted from additional fiberboard compaction during handling and transport. The as-built initial axial gap for this (or any other package) is unknown, but the nominal axial gap is specified as 0.8 inch. Changes in the fiberboard dimensions and the axial gap can occur from changes in the fiberboard moisture content, and from settling and compaction during service. Moisture accumulation in the bottom fiberboard layers can cause these layers to compress under the weight of the package internal components (shield and containment vessels) and the package contents. This is seen by comparing dimensions LH1 and LH2 in Table 1. Dimension LH1 (the full height of the lower fiberboard subassembly) is 0.722 inch below nominal, while dimension LH2 (height from the bearing plate to the lower subassembly lower step) is only 0.207 inch less than nominal. This indicates a significant reduction in height has occurred below the lower bearing plate.

Fiberboard visual appearance:

The field surveillance report included observation of dried glue residue on the upper fiberboard subassembly. Four such areas were observed during the SRNL examination, two of which are shown in Figure 1. One small (~1/4 x 1/2”) dark stain was observed on the upper fiberboard subassembly OD surface. Mold was observed on and near the bottom of the lower fiberboard subassembly (Figures 2 and 3). In addition, dark staining from moisture was observed on the lower side and bottom of the lower fiberboard subassembly.

Despite the elevated moisture concentration at the bottom of the fiberboard, gaps existed between the lower fiberboard subassembly and drum, and the lower subassembly came out smoothly without interference.

Fiberboard moisture content:

The moisture content of the fiberboard will affect its properties, including density, mechanical strength and thermal properties. Measuring the moisture content of the top and bottom subassemblies, and the relative humidity inside the package, provides reference data to potentially correlate laboratory test results with behavior in KAC. The fiberboard moisture

content was measured during the SRNL examinations. Measurements were also taken during field surveillance to the extent the fiberboard was accessible.

A GE Protimeter Surveymaster moisture probe was used to measure the moisture content of the top and bottom fiberboard subassemblies. This probe identifies the wood moisture equivalent (WME), or the weight % of moisture that would produce the same electrical conductivity in wood. Moisture content data from each examination are presented in Figure 4.

Moisture measurements were compared to those taken during previous destructive examinations. Based on the overall average moisture content, this package has a typical fiberboard moisture level. However, due to the relatively high heat load in the package, there is a concentration of moisture in the bottom fiberboard layers, similar to that observed in 9975-02101.

Consistent with recent efforts to correlate moisture content of fiberboard with humidity in the surrounding air, data were taken to correlate these two parameters. The fiberboard was placed back in the drum with a narrow channel cut down the side. A humidity probe was placed in this channel such that it could be raised and lowered with the drum closed. A plastic bag was taped over the top of the drum and sealed around the humidity probe cable. After allowing time for the humidity levels in the drum to approach equilibrium, humidity readings were taken at several elevations along the fiberboard, and the fiberboard was then removed to measure the moisture content at those same locations. The humidity data were then converted to the equivalent relative humidity corresponding to a constant temperature of 21 °C, since relative humidity is temperature dependent. These data are summarized in Figure 5, and compared to similar data from several previous DE packages and laboratory samples with cane fiberboard. The data from 9975-02019 show reasonable agreement with the other data.

Fiberboard thermal and mechanical properties:

Samples of fiberboard were removed from the bottom fiberboard subassembly to measure compressive strength, specific heat capacity and thermal conductivity. The source locations of these samples are illustrated in Figure 6. The thermal conductivity sample from the bottom center of the subassembly is oriented for heat flow in the axial direction (perpendicular to the glue joints). The thermal conductivity sample from the side is oriented for heat flow in the radial direction (parallel to the glue joints). Testing on each sample was performed at a nominal (mean) temperature of approximately 25ºC (77ºF), with no environmental conditioning. Physical data from the fiberboard samples are recorded in Table 2.

A total of four samples were prepared from the side and base of the lower subassembly for measuring the specific heat capacity of the fiberboard. The specific heat capacity was calculated in accordance with ASTM C351 at a mean temperature of ~25ºC (77ºF). This ASTM Standard specifies test temperatures that would produce a mean test temperature of 60ºC, but allows alternate test temperatures to be substituted as needed. Data were collected for a sample target temperature of 45ºC, and a water temperature of ~5ºC. The average sample moisture content was 19.2 %WME (wood moisture equivalent) for the two base samples and 9.2 %WME for the two side samples. Each sample was tested four times, and all results were averaged. The average specific heat capacity value was 1627 J/kg-K for the base samples, and 1312 J/kg-K for

the side samples. The difference in these two averages reflects the different moisture content. Multiplying the specific heat capacity by the density of the lower subassembly (298 kg/m^3) and converting units gives a heat capacity of 7.24 Btu/ft^3-F for the base samples and 5.84 Btu/ft^3-F for the side samples. This meets the required minimum value of 3 Btu/ft^3-F. The specific heat capacity value is within the range for typical baseline laboratory data, and is consistent with previous DE packages.

The thermal conductivity of the fiberboard was measured with either a Lasercomp Inc. Fox 300 or Fox 314 thermal conductivity instrument at a mean temperature of 25ºC (77ºF). For the sample with axial heat flow (perpendicular to the fiberboard layers), the measured thermal conductivity is 0.0671 W/m-K (0.0388 Btu/hr-ft-ºF) with a moisture content of 19.7 %WME. This value falls within the identified range [5], and is slightly higher than typical baseline laboratory data [10]. For the sample with radial heat flow (parallel to the fiberboard layers), the measured thermal conductivity is 0.1170 W/m-K (0.0676 Btu/hr-ft-ºF), with a typical moisture content of 10.7 %WME. Since this thermal conductivity value falls outside the identified range of 0.053 – 0.067 Btu/hr-ft-ºF [5], the test was repeated. With a slightly lower moisture content of 9.9 %WME, the thermal conductivity was 0.0657 Btu/hr-ft-ºF and falls within the identified range. Both thermal conductivity values measured in the radial orientation are slightly higher than typical baseline laboratory data [9].

The compression test data are shown in Figures 7 and 8, along with baseline data for a different fiberboard assembly. A series of photographs showing typical compression behavior under parallel loading is shown in Figure 9. The area under the stress-strain curve up to 40% strain is used as a relative indication of the energy absorption capacity of the fiberboard. This metric is shown in Figure 10 for all destructively examined packages as a function of fiberboard moisture content. In general, the energy absorption capacity decreases as the moisture content increases. The results from 9975-02019 are circled in Figure 10. These data show a trend consistent with the other DE packages.

Lead shield examination:

The entire surface of the lead shield was visually examined. It was found to be free from significant deformation and physical damage. The outer side surface is covered with white corrosion product, with varying thickness, as has been observed on other packages (Figure 11).

Several lead shield dimensions were measured (Table 3) and all are consistent with drawing requirements.

The radial thickness was measured near the top of the shield, and was calculated from diametral data taken near the bottom of the shield. The calculated thickness from near the bottom (0.538 inch) is slightly less than the measured thickness near the top (0.555 inch). This comparison is made to indicate whether the lead may have undergone creep during service; and indicates no significant creep has occurred to date.

O-ring examination and testing:

Prior surveillance testing of the four O-rings from this package included visual examination, dimensional and hardness measurements. Dimensional measurements were repeated on each O-ring as part of the destructive examination. Three of these O-rings (SCV outer, PCV outer and PCV inner) received additional testing. All three were submitted for FT-IR spectroscopy to confirm material composition, and the two outer O-rings received optical and SEM microscopic examination of the cross section. The dimensions and weight of the SCV outer and PCV outer O-rings were recorded to calculate their density. The PCV inner O-ring was tensile tested, including a hold point at 50% strain to visually examine the O-ring.

Weight and dimension data for the two outer O-rings are presented in Table 4. The average minor diameter for each O-ring is within the specified tolerances for new O-rings, but the major inside diameter for each O-ring (calculated from the length measured after the O-ring was cut) is greater than specified for new O-rings. This is consistent with a permanent stretch due to the lid diameter. Leak testing during the field surveillance successfully demonstrated leak-tightness to a level of approximately 1×10^{-3} std cc air/sec.

Compression set was calculated for each O-ring based on each of the dimensional measurements it received. Compression set is calculated as follows, assuming an initial minor diameter of 0.139 inch and an average groove depth in the lid of 0.0995 inch.

$$\text{Compression set (\%)} = (0.139 - \text{radial thickness}) / (0.139 - 0.0995)*100$$

Compression set for the 9975-02019 O-rings ranged from 35 to 41% based on KAC measurements. The compression set decreases with time, as the polymer continues to relax. Typically, the compression set has reached an equilibrium value after about 30 days. When measured in SRNL 28 days later, the compression set ranged from 4 to 17%. Individual readings were consistent for the KAC measurements, but varied significantly for the SRNL measurements, suggesting the O-rings had twisted after the KAC measurements. The compression set values are generally consistent with the range of values measured for O-rings from other packages.

FT-IR spectroscopy generically identified the composition of each O-ring as consistent with a Viton® type fluoroelastomer (Figure 12). Each O-ring produced a similar FTIR spectrum consistent with that from previous characterization of Viton® GLT O-rings, and with a library image of a Viton® FTIR spectrum.

As with previous destructive examinations, visual (Figure 13) and SEM (Figure 14) examination of the cross sections identified a distribution of very small particles throughout each O-ring. Aside from carbon and fluorine (the primary constituents of Viton® fluoroelastomer) the SEM identified small amounts of zinc, aluminum and silicon. Though the actual compound is proprietary, Viton®-type fluoroelastomer compounds typically contain MgO, CaO, $Ca(OH)_2$, ZnO or lead compounds as acid acceptors and heat stabilizers [10]. Aluminum is present in hydrotalcite, which is used in both GLT and GLT-S compounds as a filler reinforcing agent. Silicon may be present as a trace contaminant.

The PCV inner O-ring was tensile tested in accordance with ASTM D1414, using a cut (single strand) sample. The test was interrupted at 50% strain (Figure 15) to visually examine the O-ring for signs of cracking or other degradation. None were observed. The initial stress-strain curve for the PCV inner O-ring is shown in Figure 16, along with results of other tests with Viton GLT O-rings. In this first test, the O-ring failed after reaching 398% elongation. A re-test was performed with a different grip arrangement, and reached 157% elongation (Figure 17). The first test uses a yarn grip which would allow some stretch beyond the gage section, especially if the O-ring had any residual grease. To more accurately measure the elongation, the second test was performed with an alternate grip arrangement which does not allow such stretch. Since these alternate flat grips pose a greater risk of breaking within the grips (which would invalidate the test), the portion of O-ring within the grips was wrapped with tape for cushioning.

General:

A general visual examination was performed on all metallic components. No significant damage or degradation of the containment vessels was observed. A dark spot was observed on the PCV top flange OD surface. This is assumed to be a rub mark, since there is a corresponding mark on the SCV ID surface (Figure 18). Both of these spots display coloration that could be indicative of light corrosion. Various fabrication markings were stamped or engraved on the containment vessels and lids. These markings appear to be identification numbers used during manufacture, prior to association of the parts with a final package number, and are consistent with those seen in other packages.

Numerous small spots of corrosion were observed along the bottom (underside) edge of the drum (Figure 19a). Similar corrosion has also been observed in this location on other packages. However, no corrosion was observed on the interior surface immediately opposite these spots (Figure 19b). Nor was any corrosion observed along the stitch welds around the bottom side of the drum. Therefore, it is unlikely that the corrosion on the bottom was driven by chlorides or other compounds leaking from the drum. Rather, it is judged that corrosion in this area results from the ambient storage environment, with influence from fabrication stresses, and the possible use of carbon steel tooling. While this corrosion, in the extreme, could lead to penetration of the drum, it currently appears to not compromise the overall integrity of the drum. In addition, the interior side of the drum had regions of staining or possible superficial corrosion (Figure 20).

The data from the examination activities described above are compared with field surveillance data in Attachment 1. There is general agreement between the two examinations, although some differences are to be expected as moisture re-distributes within the fiberboard and the O-rings slowly relax. All findings will be reviewed by NMM for potential impact on the continued storage of other packages in KAC.

Measurement Uncertainties:

Numerous measurements were made with a variety of instruments during the destructive examination of package 9975-02019. Some of the measurements were specifically compared to inspection criteria, while others were taken for information / trending purposes. All

measurements which are compared to inspection criteria were made with calibrated instruments, or were verified against calibrated instruments. The uncertainties associated with measurements and calculated results required to meet inspection criteria are discussed below.

Weight – The weight of each fiberboard subassembly was measured to a precision of 1 gram. The balance used was M&TE, and the calibration data show accuracy within 5 grams over the range of interest. A conservative net uncertainty of 6 grams will be used.

Calipers – Three different calipers were used to measure component dimensions. All three calipers are M&TE, and calibration data show accuracy within 0.001 inch. In addition, operator bias can affect measurement accuracy through the contact load applied when making a measurement. A degree of give exhibited by the fiberboard will lead to different results as the contact load changes. The larger calipers are judged to be more susceptible to this bias. Metallic components are significantly more rigid than the fiberboard, but operator bias may also exist for those components. While not characterized explicitly, it is judged that the total uncertainty (instrument uncertainty plus operator bias) for fiberboard measurements is no greater than +/- 0.003 inch for the 6 inch calipers, +/- 0.005 inch for the 24 inch calipers, and +/- 0.007 inch for the 40 inch calipers. It is further judged that total uncertainty when measuring metallic components is no greater than +/- 0.003 inch for 6 and 24 inch calipers, and +/- 0.005 inch for the 40 inch calipers.

Manual calipers – Dimension ID2 on the lead shield was captured with manual swing calipers, which was then locked to that dimension and measured with 24-inch calipers. It is judged that the accuracy of capturing this dimension with the manual calipers is within +/- 0.002 inch, and the measurement of that dimension is then within +/- 0.002 inch, for a (conservatively) combined accuracy of +/- 0.004 inch.

Thermal conductivity instrument – The specifications for the Fox300 and Fox 314 thermal conductivity instruments include a stated accuracy of ~1% and 2%, respectively. Measurement of the thermal conductivity of a calibration standard was accurate to within 1.1% on either instrument. An uncertainty of 3% will be conservatively assumed for the current measurements on either instrument.

Heat capacity – The specific heat capacity is derived from temperature and weight measurements, using calibrated instruments. The thermocouple and balance precisions are high. The greatest contribution to error in the specific heat capacity is considered to be consistency of operator technique. The total uncertainty is reflected in the range of results for multiple trials. The heat capacity was reported separately for the base and side regions, with four measurements on each of two samples from each region. The variation for each sample ranged from 9.8 to 25.2%. The combined uncertainty on the average of 2 samples is 7.5% for the base region, and 15.9% for the side region.

Where measurement results are used in subsequent calculations, the uncertainty values identified above are assumed to be random. A standard error propagation formula for random errors is used to calculate the final result uncertainty. In some cases, the calculated uncertainty may be less than the potential error from rounding off the result, and the higher variation associated with

round-off is reported as the uncertainty. These calculations are documented in the Laboratory Notebook [8]. Calculation results and their uncertainties are summarized as follows:

- Top fiberboard subassembly volume = 28216 +/- 26 cm^3
- Top fiberboard subassembly density = 0.273 +/- 0.001 g/ cm^3
- Bottom fiberboard subassembly volume = 83372 +/- 71 cm^3
- Bottom fiberboard subassembly density = 0.299 +/- 0.001 g/ cm^3
- Shield radial thickness at bottom = 0.538 +/- 0.003 inch
- Thermal conductivity (radial) = 0.0657 +/- 0.002 Btu/hr-ft-ºF
- Thermal conductivity (axial) = 0.0388 +/- 0.001 Btu/hr-ft-ºF
- Heat capacity = 5.8 +/- 0.9 Btu/ft^3-ºF (side), 7.2 +/- 0.5 Btu/ft^3-ºF (base)

References

[1] WSRC-SA-2002-00005, Rev. 10, "K-Area Material Storage Facility Documented Safety Analysis", October 2014.

[2] SRNS-STI-2010-00763 Rev. 0, "9975 Shipping Package Life Extension Surveillance Program Results Summary", W. L. Daugherty, K. A. Dunn, E. R. Hackney, E. N. Hoffman and T. E. Skidmore, January 2011.

[3] SRNS-TR-2008-00290, Revision 1, Summary and Matrix for the 9975 Shipping Package Qualification Programs for Extended Storage of Plutonium in the K-Area Complex (U), April 2011

[4] WSRC-TR-2001-0286, Rev. 7, "The Savannah River Site Surveillance Program for the Storage of 9975/3013 Plutonium Packages in KAC", January 2015

[5] WSRC-TR-2005-00135 Rev. 1, "Task Technical and Quality Assurance Plan for Destructive Examination of a 9975 Package from Field Surveillance Activities", W. L. Daugherty, March 2011

[6] WSRC-TR-2004-00197, "Inspection Activities and Acceptance Criteria for Field Surveillance of Model 9975 Package O-Rings and Celotex® Materials", W. L. Daugherty, April 2004

[7] SOP-CSS-232-K, Rev. 2, Attachment 8.5 "3013/9975 Surveillance Data Sheet" for 9975-02019

[8] SRNL-NB-2012-00048, Laboratory Notebook "9975 Shipping Package Celotex Testing Book IV

[9] SRNL-STI-2015-00610, "Status Report – Cane Fiberboard Properties and Degradation Rates for Storage of the 9975 Shipping Package in KAC", W. L. Daugherty, December 2015

[10] Rubber Technology Handbook, W. Hofmann, Hanser Publishers, New York, 1989, page 122

Table 1. Fiberboard physical measurements and calculated density

Upper Subassembly						
Weight	12.129 kg					R-R2-F-0019 Rev 5
	0/180 deg.		90/270 deg.		Avg.	Nominal value (inch)
UD1 (in)	17.660		17.654		17.657	17.7
UD2 (in)	8.566		8.562		8.564	8.55
	0 deg.	90 deg.	180 deg.	270 deg.	Avg.	
UR1 (in)	3.043	3.028	3.037	3.027	3.034	3.075
UR2 (in)	1.481	1.495	1.520	1.474	1.492	1.5
UH1 (in)	7.042	7.072	7.063	7.068	7.061	7.1
UH2 (in)	2.068	2.082	2.087	2.059	2.074	2.1
UH3 (in)	4.954	4.957	4.966	4.976	4.963	5.0

Upper subassembly calculated density = 0.273 g/cc

Lower Subassembly						
Weight	27.078 kg					R-R2-F-0019 Rev 5
	0/180 deg.		90/270 deg.		Avg.	Nominal value (inch)
LD1 (in)	18.048		18.050		18.049	18.1
LD2 (in)	8.496		8.502		8.499	8.45
	0 deg.	90 deg.	180 deg.	270 deg.	Avg.	
LR1 (in)	3.235	3.256	3.214	3.215	3.230	3.275
LR2 (in)	1.515	1.501	1.504	1.497	1.504	1.55
LH1 (in)	25.938	25.937	26.025	26.013	25.978	26.7
LH2 (in)	20.185	20.192	20.198	20.198	20.193	20.4
LH3 (in)	2.014	2.008	2.008	2.013	2.011	2.0

Lower subassembly calculated density = 0.299 g/cc

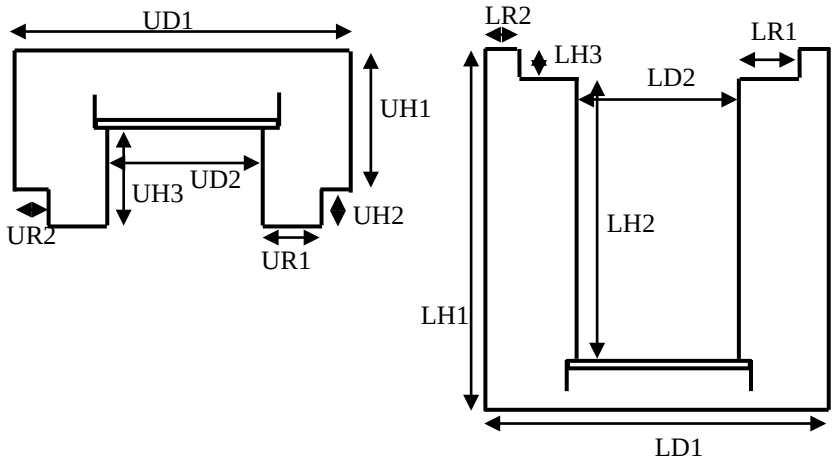

Table 2. Physical data for fiberboard test specimens

Test Sample	Moisture Content (%WME)	Weight (g)	Length (inch)	Width (inch)	Height (inch)	Density (g/cc)
Compression Test Samples						
Side 1 (parallel)	9.4	36.222	2.027	1.989	1.959	0.280
Side 2 (parallel)	9.5	37.767	2.033	1.998	2.024	0.280
Side 3 (perpendicular)	9.1	37.473	2.030	2.008	2.014	0.279
Side 4 (perpendicular)	9.3	38.104	2.023	2.028	2.012	0.282
Base 1 (parallel)	20.8	35.964	2.019	1.993	2.019	0.270
Base 2 (parallel)	23.5	35.138	2.012	1.968	2.006	0.270
Base 3 (perpendicular)	20.4	35.602	2.014	2.002	2.024	0.266
Base 4 (perpendicular)	21.0	35.231	1.992	2.008	2.016	0.267
Thermal Conductivity Samples						
Side (radial) *	10.7 9.9	380 378	7.028 6.977	6.984 6.971	1.635 1.643	0.289 0.289
Base (axial)	19.7	314	6.978	6.968	1.446	0.273

* Data provided for the radial thermal conductivity sample as-machined, and after drying slightly.

Table 3. Lead shield dimensions

Dimension	0/180 deg. (inch)		90/270 deg. (inch)		Avg. (inch)	Requirement (inch)
OD (in)	8.333		8.332		8.332	8.252 – 8.35
ID1 (in)	7.276		7.262		7.269*	7.25 – 7.26
ID2 (in)	7.260		7.250		7.255	7.24 – 7.26
	0 deg.	90 deg.	180 deg.	270 deg.		
R (in)	0.550	0.563	0.550	0.558	0.555	0.506 min
H (in)	24.680	24.678	24.685	24.674	24.679	24.556 – 24.7

(OD – ID2) / 2 = 0.538 inch

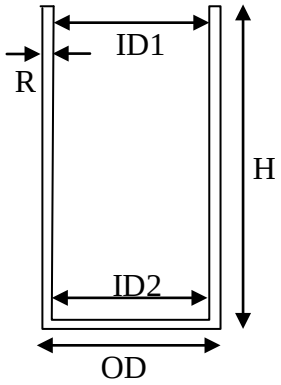

* ID1 re-measured at 4 locations, average value = 7.26 inch

Table 4. O-ring physical data

~28 Days after Field Surveillance	PCV Outer O-Ring Thickness		SCV Outer O-Ring Thickness	
	Radial (inch)	Axial (inch)	Radial (inch)	Axial (inch)
Minor Dia. 0 deg	0.1425	0.1345	0.1325	0.1390
Minor Dia. 45 deg	0.1415	0.1350	0.1365	0.1370
Minor Dia. 90 deg	0.1360	0.1350	0.1305	0.1375
Minor Dia. 135 deg	0.1295	0.1350	0.1330	0.1380
Minor Dia. 180 deg	0.1290	0.1355	0.1320	0.1370
Minor Dia. 225 deg	0.1285	0.1350	0.1310	0.1370
Minor Dia. 270 deg	0.1305	0.1345	0.1320	0.1375
Minor Dia. 315 deg	0.1405	0.1320	0.1310	0.1370
Avg. Minor Dia.	**0.1347**		**0.1349**	
Minor Dia. (new)	0.138 +/- 0.006 inch		0.138 +/- 0.006 inch	
Length (after cut)	14 7/32 inch		17 15/32 inch	
Calculated Major Dia.	4.526 inch avg		5.561 inch avg.	
Major Inside Dia. (new)	4.234 +/- 0.030 inch		5.234 +/- 0.035 inch	
Weight	5.9330 g		7.4625 g	
Calculated Volume	0.203 $inch^3$ (3.320 cm^3)		0.250 $inch^3$ (4.092 cm^3)	
Calculated Density	**1.787 g/cm^3**		**1.824 g/cm^3**	


(a)


(b)

Figure 1. Two of the regions of the upper fiberboard subassembly with smeared glue.

(a) (b)

Figure 2. Mold on the side of the lower fiberboard subassembly

Figure 3. Mold and dark staining on the bottom of the lower fiberboard subassembly.

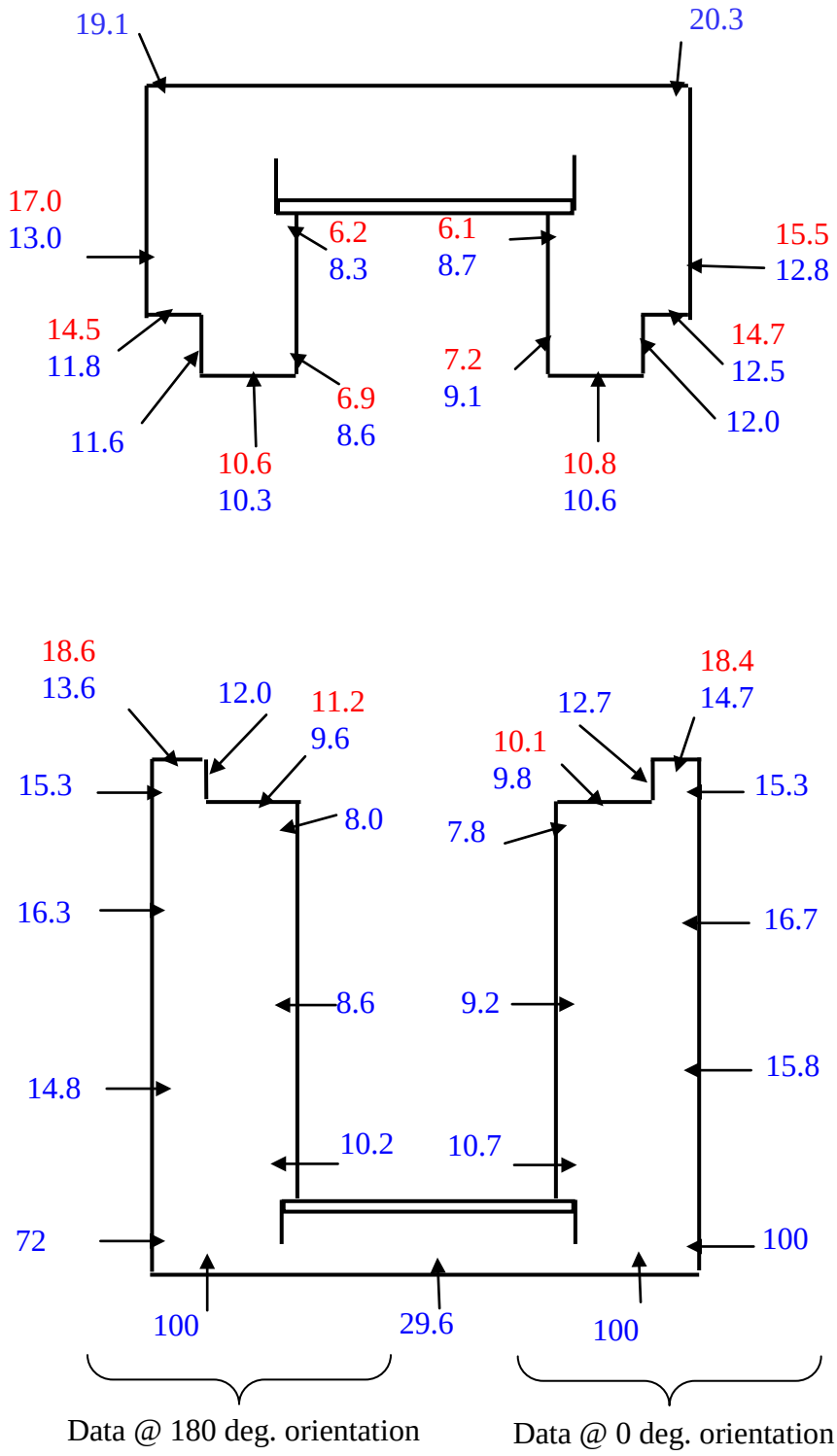

Figure 4. Fiberboard moisture content data. The values in red were measured during field surveillance. The values in blue were measured 15 days later, except for the top of the upper fiberboard subassembly which was measured 21 days later. All values are % wood moisture equivalent.

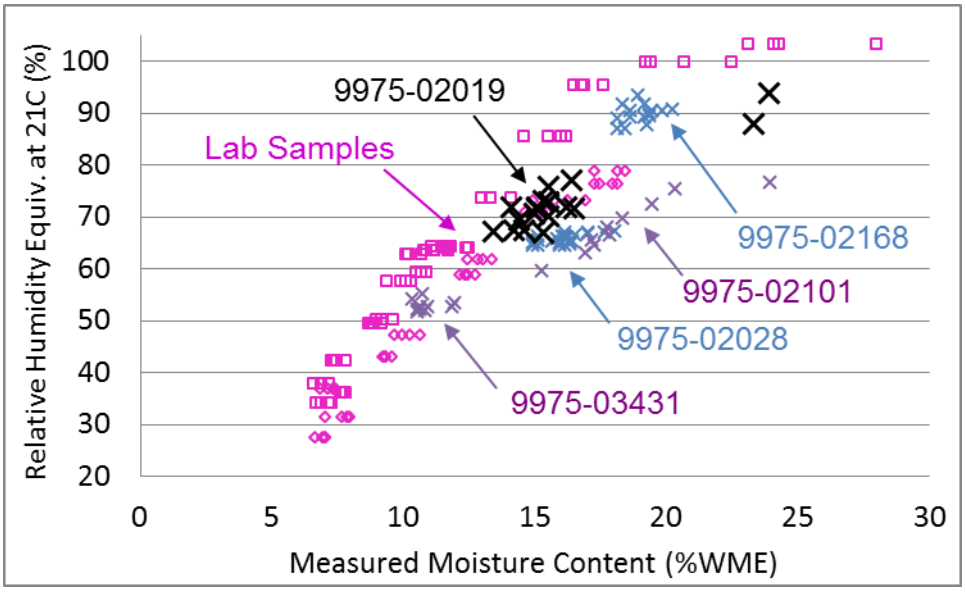

Figure 5. Correlation between fiberboard moisture content and relative humidity of the adjacent air. Data from 9975-02019 are shown with comparable data from prior cane fiberboard DE packages and laboratory samples. Measurements were taken along the fiberboard OD surface. Since relative humidity is temperature dependent, all the data in this graph have been converted to a consistent equivalent relative humidity at 21 °C.

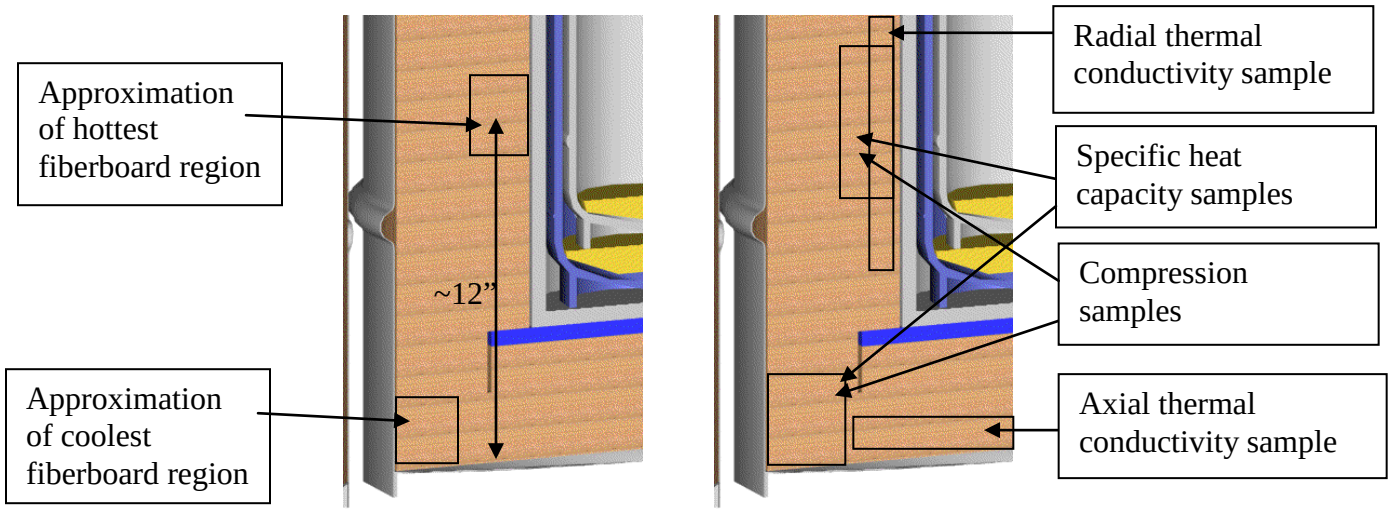

Figure 6. Illustration of fiberboard regions of the lower subassembly to be tested. Multiple samples (where used) were removed from the illustrated locations at different circumferential positions. Not to scale.

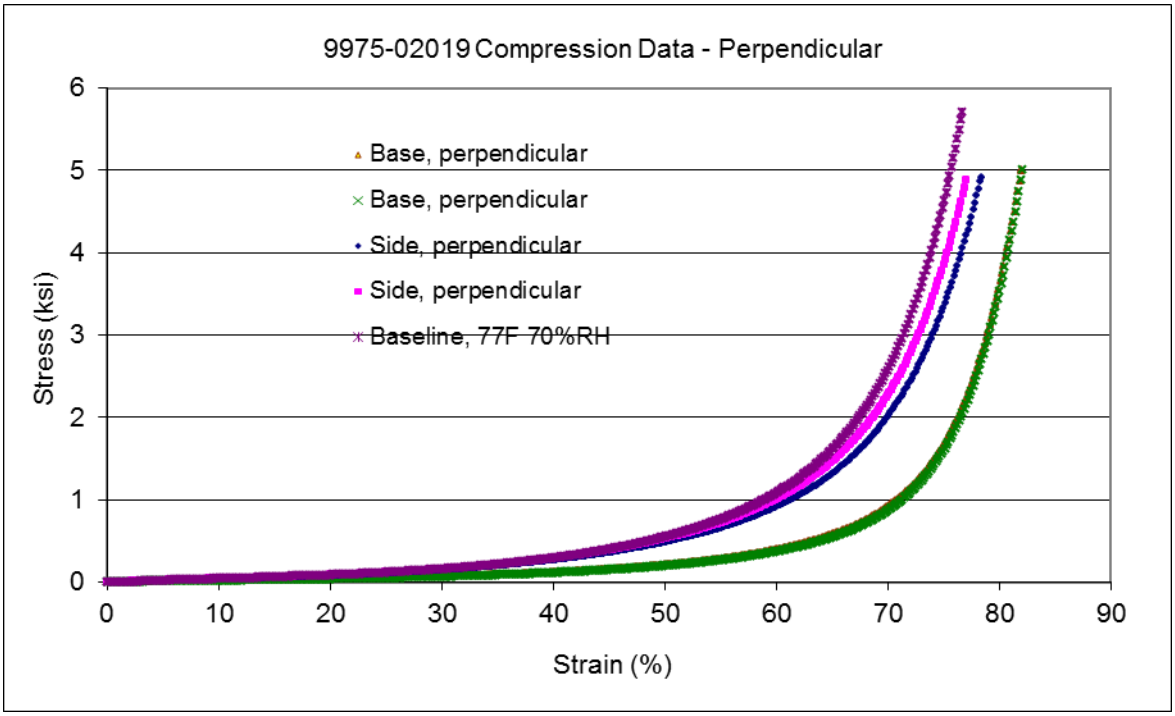

Figure 7. Fiberboard compression test data, compared with typical baseline data from an unaged assembly, in the perpendicular orientation (i.e. load applied perpendicular to the fiberboard layers).

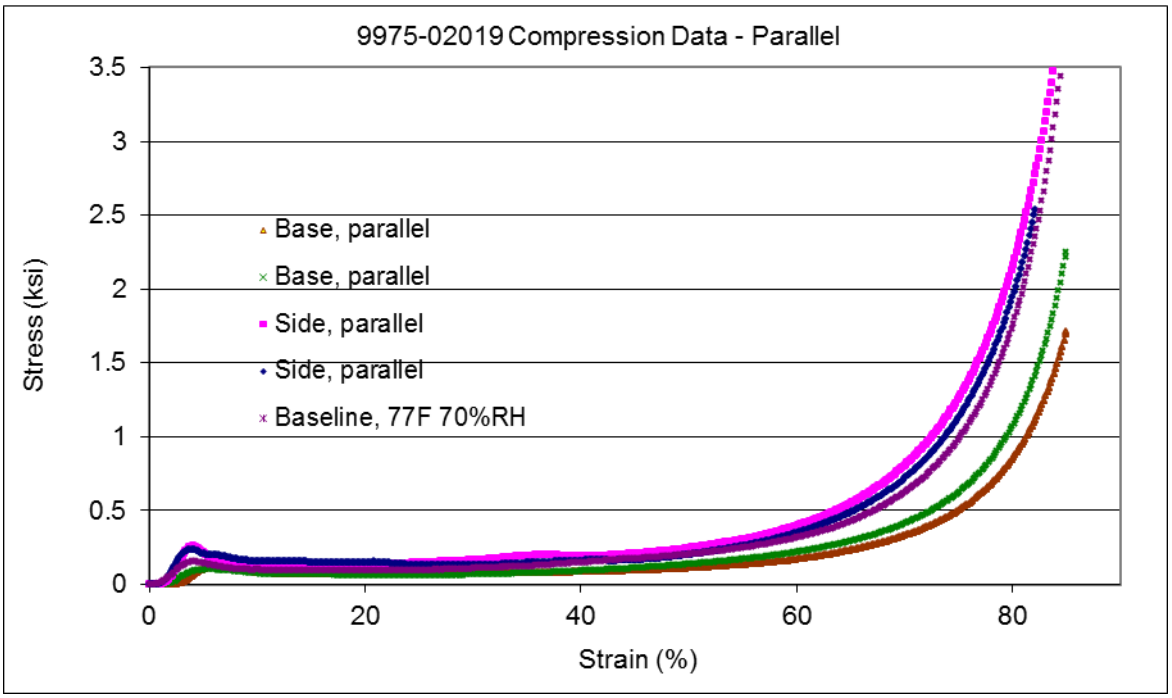

(a)

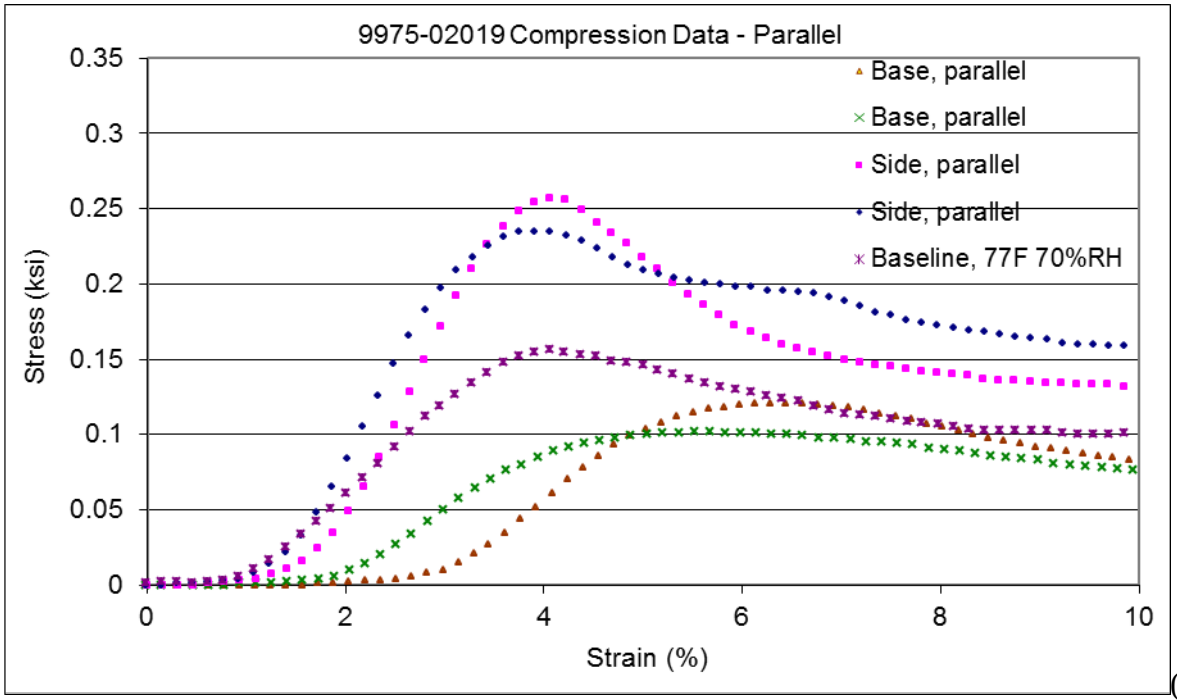

(b)

Figure 8. Fiberboard compression test data, compared with typical baseline data from an unaged assembly, in the parallel orientation (i.e. load applied parallel to the fiberboard layers). The full curves are shown in (a), while the initial buckling region is expanded in (b).

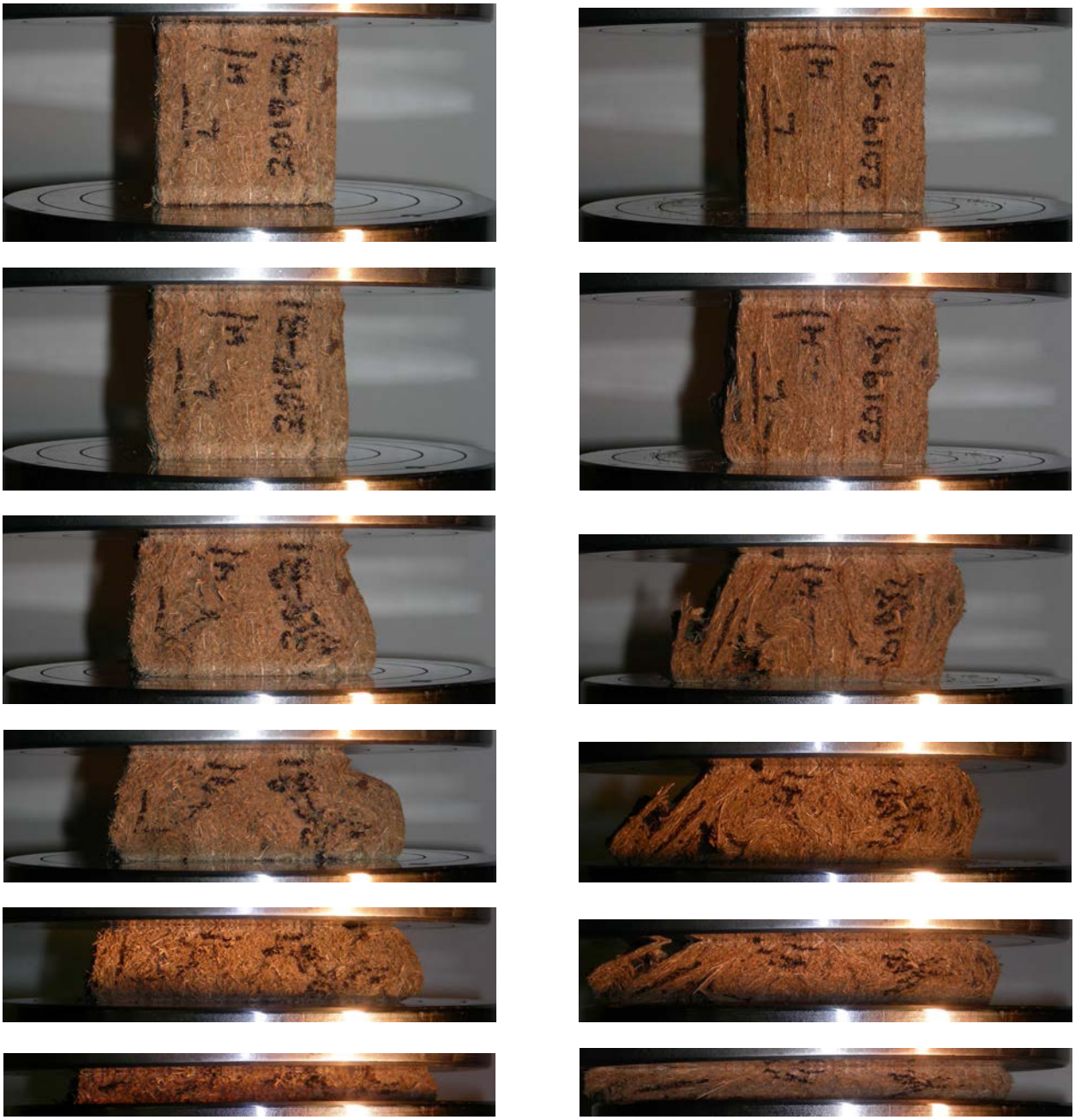

(a) Sample B1 from base of subassembly (b) Sample S1 from side of subassembly

Figure 9. Photographs of fiberboard samples during compression testing, parallel orientation

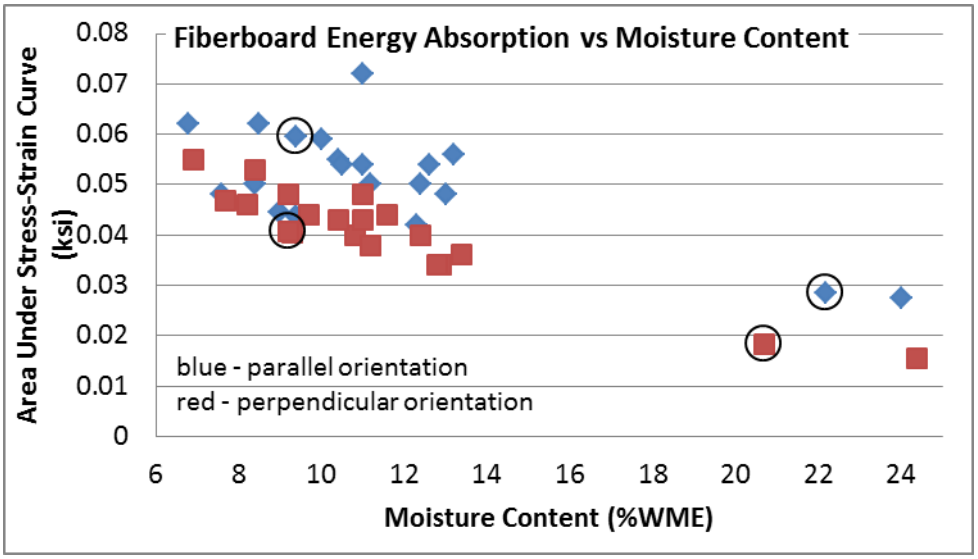

Figure 10. Fiberboard energy absorption, represented by the area under the stress-strain curve up to 40% strain, from tensile test samples from all destructively examined packages. The results from 9975-02019 are circled.

(a) side view

(b) bottom view

Figure 11. Lead shield with white corrosion product.

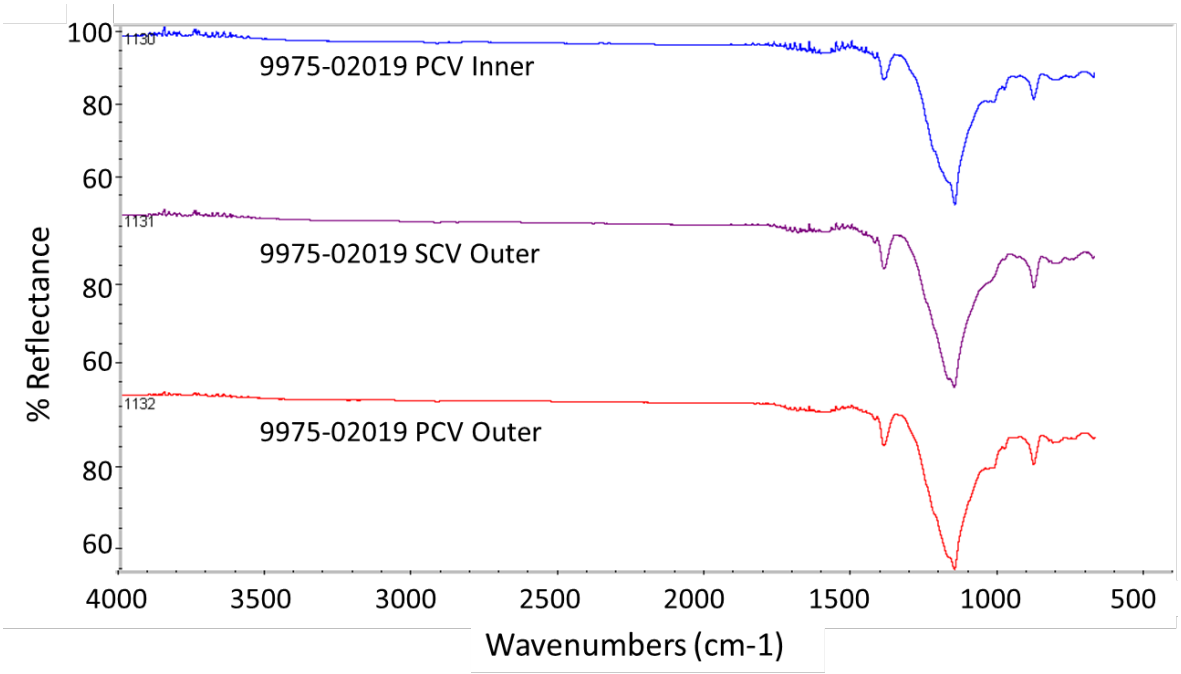

Figure 12. FT-IR spectra for the three tested Viton® GLT O-rings from 9975-02019. PCV outer – red, PCV inner – blue, SCV outer – purple.

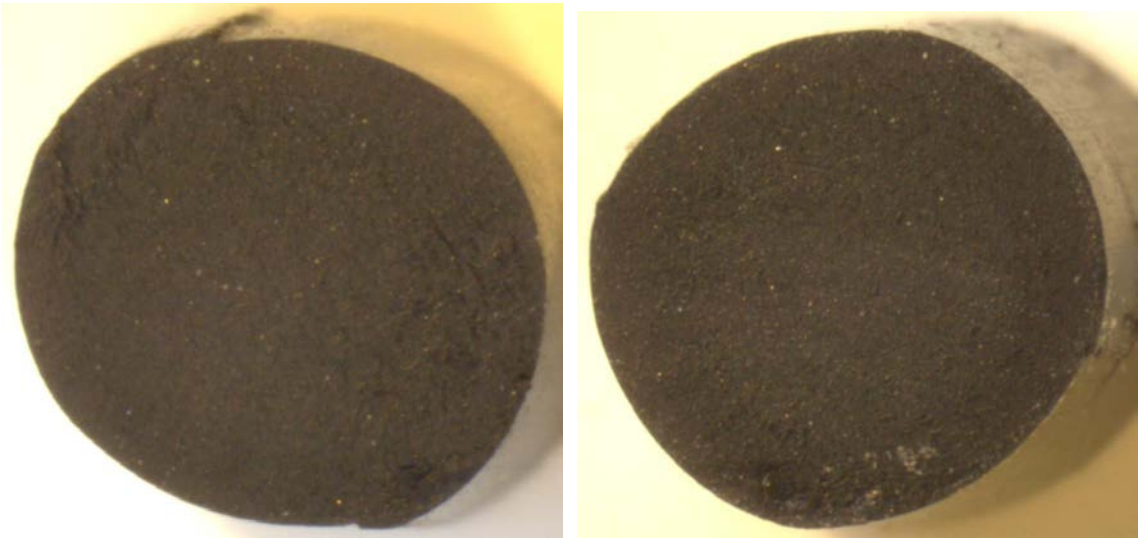

(a) (b)

Figure 13. Optical cross section of the (a) PCV outer and (b) SCV outer O-rings. Photos taken by 723-A Met Lab.

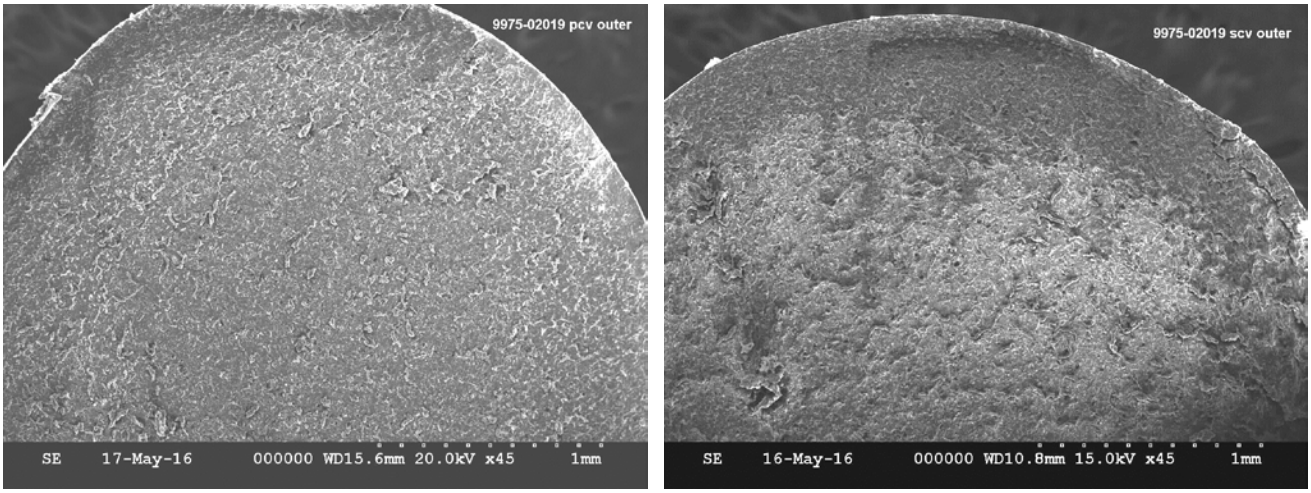

(a) (b)

Figure 14. SEM cross section of the (a) PCV outer and (b) SCV outer O-rings. Photos taken by 723-A Met Lab.

(a) With yarn grips (b) with flat grips

Figure 15. 9975-02019 PCV inner O-ring during tensile test, at 50% stretch.

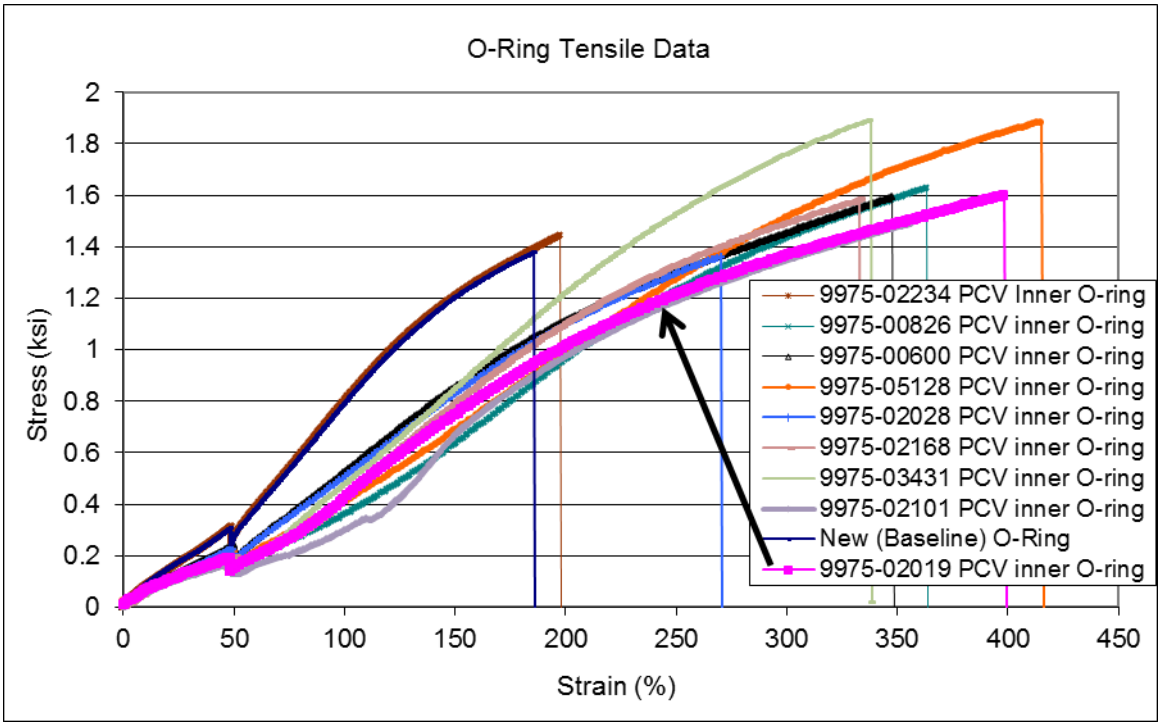

Figure 16. Tensile data for PCV inner O-ring from 9975-02019, with comparison curves from other DE packages with Viton GLT O-rings. All of these tests were conducted with the original yarn grip configuration

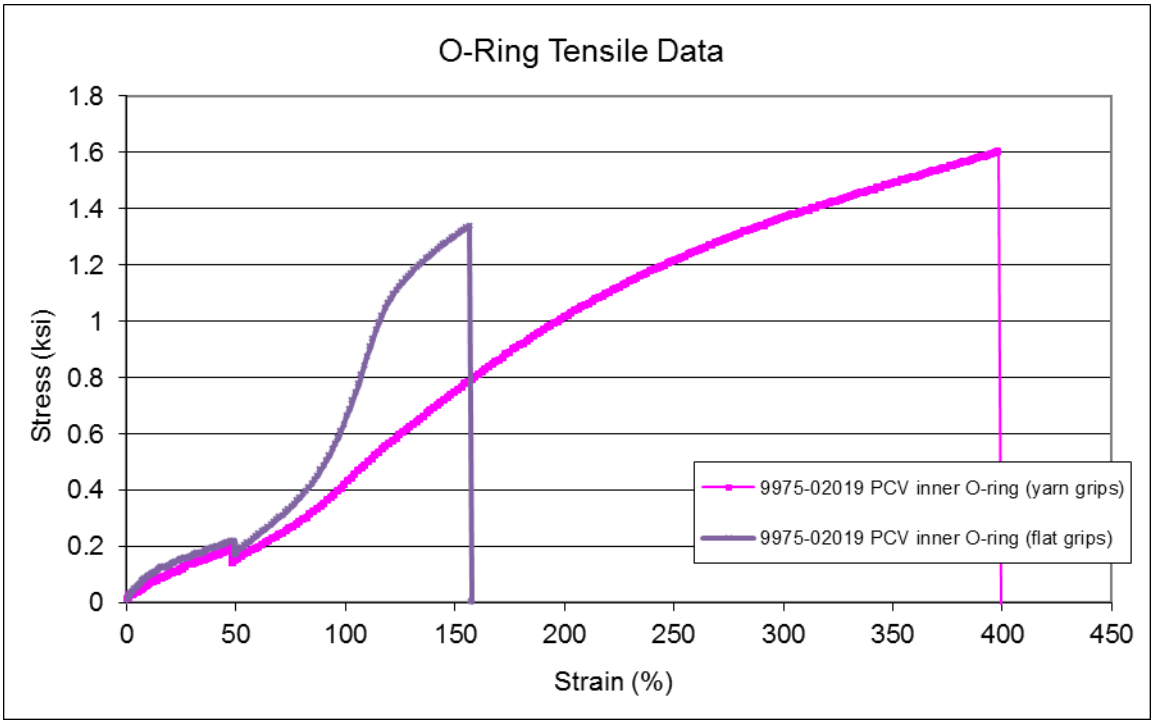

Figure 17. Tensile data for PCV inner O-ring from 9975-02019 comparing effect of yarn grips and flat grips.

(a) (b)

Figure 18. Rub marks, with possible light corrosion, on the PCV flange (a) and SCV interior (b)

(a) Exterior view

(b) Corresponding interior view

Figure 19. Areas of corrosion on the drum exterior bottom along the outer corner (a). The corresponding interior region (b) shows some rub marks, but is not corroded.

Figure 20. Region of staining and/or superficial corrosion on the drum interior

Attachment 1 9975-06100 Field Surveillance Results, with Comparison to Destructive Examination Results

Section I

Drum Exterior Examination

Item	Field Surveillance Result	Destructive Exam. Result
Drum vent plugs are specified and are in place as required	SAT	SAT
Drum surface is not dented beyond 0.25 inch	SAT	SAT
Drum Dents adjacent to the air shield are not deeper than 0.125 inch	SAT	SAT
Drum surface is free from corrosion, swelling/bulging and other physical damage	SAT	UNSAT

Comment – Numerous small corrosion spots along edge on the bottom of drum (exterior) during DE exam.

Section II

Humidity Measurements

Humidity at top of the drum	89.5 %RH	50.4 %RH on 4/20/16

Section III

Temperature Measurements

[These data not repeated in this report.]

Section IV

Celotex® Inspection

Upper Celotex® Assembly Weight: 26.8 lb (field surv.) 12.129 kg / 26.74 lb (destructive exam)

Visual:

Item	Field Surveillance Result	Destructive Exam. Result
Inspect all exposed Celotex® surfaces for significant damage and ensure layers are well bonded	SAT	SAT
Upper Celotex® came out smoothly, without interference	SAT	SAT
All visible Celotex® surfaces are free from staining and variation in coloration	UNSAT	UNSAT
Celotex® is free from significant swelling (e.g. gap exists against drum), shrinkage and other significant physical damage	SAT	SAT
Lead shield is free from significant deformation and physical damage and shows no sign of flaking, blistering or spalling	SAT	SAT
Lead shield Go/No Go gauge went smoothly into the lead shield and reached all the way to the bottom of the lead shield	SAT	NA

Comments: From field surveillance, “Dried (hard, crusty) glue @ two areas of upper celotex” From DE: “Upper fiberboard assembly – dark stains from smeared glue, plus 1 small (~1/4 x ½”) dark stain on OD surface @ ~130°. Lower fiberboard assembly – mold on side and bottom, dark stains (saturated) on lower side and bottom.”

Attachment 1 9975-06100 Field Surveillance Results, with Comparison to Destructive Examination Results

Celotex® Dimensions (all results reported in inches)

Dimensions		0°	90°	180°	270°	Field Surveillance Average	Destructive Exam. Average
1	Upper Assembly OD	17.604	17.639			17.622	17.657
2	Upper Assembly lower step OD	14.636	14.656			14.646	14.632*
3	Upper Assembly ID	8.536	8.538			8.537	8.564
4	Upper Assembly inside height	4.933	4.958	4.959	4.933	4.946	4.963
5	Lower Assembly step height	2.024	1.976	2.025	2.014	2.010	2.011
6	Lower Assembly height from lower step to top of lead shield	4.472	4.473	4.511	4.514	4.493	NA

* calculated value

Dimension	Result	Criteria	Field Surveillance Result	Destructive Exam. Result
Dimension #4 average – Dimension #6 average	0.453	>0.425”	SAT	NA
Dimension #6 average	4.493	$\leq$ 4.65 ”	SAT	NA
Dimension #1 average – Dimension #3 average	9.085	$\geq 8\ ^{3/16}$ ”	SAT	SAT

Section V

O-Ring Inspection

Test	SAT/UNSAT
O-ring seal test performed on SCV	SAT
SCV O-rings were removed intact	SAT
SCV O-rings have no excess accumulation of grease	SAT
O-ring seal test performed on PCV	SAT
PCV O-rings were removed intact	SAT
PCV O-rings have no excess accumulation of grease	SAT

Comments: n/a

Attachment 1 9975-06100 Field Surveillance Results, with Comparison to Destructive Examination Results

(all dimensional results reported in inches)

Action	0°	90°	180°	270°	Time	Destructive Exam. Average Result
Loosen SCV lid					1003	NA
Outer SCV O-Ring						
Measure OD (while on plug)	6.264	6.278			1006	NA
Measure radial thickness	0.1245	0.1235	0.1255	0.1245	1011	0.1323
Measure vertical thickness	0.1375				1010	0.1375
Inner SCV O-Ring						
Measure OD (while on plug)	6.173	6.178			1008	NA
Measure radial thickness	0.1235	0.1245	0.1265	0.1260	1010	0.1373
Measure vertical thickness	0.1360				1009	0.1348
Loosen PCV lid					1018	NA
Outer PCV O-Ring						
Measure OD (while on plug)	5.232	5.240			1020	NA
Measure radial thickness	0.1215	0.1240	0.1220	0.1240	1023	0.1348
Measure vertical thickness	0.1350				1023	0.1346
Inner PCV O-Ring						
Measure OD (while on plug)	5.122	5.123			1021	NA
Measure radial thickness	0.1250	0.1260	0.1255	0.1245	1023	0.1351
Measure vertical thickness	0.1350				1022	0.1332

Attachment 1 9975-06100 Field Surveillance Results, with Comparison to Destructive Examination Results

SRNL Receipt Examination of O-Rings

VISUAL EXAMINATION

PCV	PCV Outer	PCV Inner
Grease present	yes	yes
Color (normal or explain)	Normal	Normal
Cross-sectional shape	round	round
Nicks, Scratches, Cracks	none	none
Other Damage (Note extent/size)	none	silvery blurs, could possibly be oxidation
Picture (Note if taken)		

SCV	SCV Outer	SCV Inner
Grease present	yes	yes
Color (normal or explain)	Normal	Normal
Cross-sectional shape	round	round
Nicks, Scratches, Cracks	none	none
Other Damage (Note extent/size)	none	none
Picture (Note if taken)		

THICKNESS (all results reported in inches)

PCV	PCV Outer		PCV Inner	
	Axial	Radial	Axial	Radial
Thickness 1 (in)	0.1305	0.1390	0.1330	0.1340
Thickness 2 (in)	0.1345	0.1300	0.1360	0.1310
Thickness 3 (in)	0.1350	0.1280	0.1380	0.1350
Thickness 4 (in)	0.1290	0.1380	0.1365	0.1285
Field Surv. Average	**0.1323**	**0.1338**	**0.1359**	**0.1321**
Destructive Exam Average	**0.1346**	**0.1348**		

SCV	SCV Outer		SCV Inner	
	Axial	Radial	Axial	Radial
Thickness 1 (in)	0.1385	0.1320	0.1370	0.1385
Thickness 2 (in)	0.1375	0.1295	0.1310	0.1340
Thickness 3 (in)	0.1370	0.1285	0.1315	0.1375
Thickness 4 (in)	0.1370	0.1305	0.1295	0.1395
Field Surv. Average	**0.1375**	**0.1301**	**0.1323**	**0.1374**
Destructive Exam Average	**0.1375**	**0.1323**		

Attachment 1 9975-06100 Field Surveillance Results, with Comparison to Destructive Examination Results

SRNL Receipt Examination of O-Rings (Continued)

HARDNESS

	PCV O-Rings		SCV O-Rings	
	Outer	Inner	Outer	Inner
Hardness 1, M-Scale	77.0	77.0	75.0	77.0
Hardness 2, M-Scale	74.0	77.5	76.0	77.0
Hardness 3, M-Scale	74.0	74.0	73.0	74.0
Hardness 4, M-Scale	77.0	78.0	74.0	76.5
Hardness 5, M-Scale	77.5	79.0	72.5	75.0
Average	**75.9**	**77.1**	**74.1**	**75.9**

CONTINUATION:
NA

CC: R. J. Bayer, 705-K
J. S. Bellamy, 730-A
W. L. Daugherty, 773-A
K. A. Dunn, 773-41A
B. A. Eberhard, 705-K
B. L. Garcia-Diaz, 999-2W
L. F. Gelder, 999-W
T. W. Griffin, 705-K
T. J. Grim, 105-K
E. R. Hackney, 705-K
E. V. Henderson, 705-K
S. J. Hensel, 705-K
J. M. Jordan, 705-K
B. B. Kiflu, 705-K
D. R. Leduc, 730-A
J. W. McEvoy, 707-C
T. E. Skidmore, 730-A
D. E. Welliver, 705-K
K. E. Zeigler, 773-41A
Document Control